

Supporting information

Handle with care! On isothermality in some commonly used plug flow reactors for X-ray based investigations of catalysts.

Mark A. Newton, Stefano Checchia, Amy. J. Knorpp, Dragos Stoian, Wouter van Beek, Hermann Emerich, Alessandro Longo, Jeroen A. van Bokhoven

1. Materials used.

The synthesis and characterisation of the Cu/MOR sample used in this study is fully described elsewhere. (ref. [30] main paper) Briefly a commercial MOR (CBV10A, Zeolyst, $\text{SiO}_2/\text{Al}_2\text{O}_3 = 13$, Na form) was copper exchanged (using copper (II) nitrate, trihydrate) overnight at 323 K then rinsed with deionised water. This process was repeated twice before the material was calcined in air at 773 K. The resulting samples was then characterized using elemental analysis, X-ray diffraction, and BET.

2. Synchrotron based measurements and activation/reaction protocols

X-ray experiments were carried out at both the Swiss Norwegian beamlines (BM31) [S1] and Dutch-Belgian beamline (DUBBLE, BM26A) [S2] at the European synchrotron radiation source. All data was collected using Si (111) monochromator systems and ionization chambers for normalization of the beam, sample data collection, and energy calibration (Cu foil). The time resolution per XANES spectrum varied between 30 s^{-1} (BM 31, SNBL) – 240 seconds (DUBBLE).

Uni-directional air blower systems were made available by both beamlines. At SNBL the set-point temperatures used were based upon a previously made (thermocouple based) calibration of the

system. At SNBL the temperature is measured and set by a thermocouple inside the blower. A previously made temperature calibration curve measured at the sample position was used for determination and correction of the temperature offset. At DUBBLE, a type-K thermocouple was inserted directly into the outlet bed of the sample bed to set the temperatures required for experimentation.

To contrast with the the uni-directional reactor systems a modified version of the plug-flow reactor system developed by Chupas and co-workers for total X-ray scattering measurements [ref. [22] main paper] was constructed and characterized at ETH and the ESRF before implementation for these types of measurement. The major modification made to the original design was the incorporation of a stainless steel bracket, with 1/8" Swagelok fittings, into which the capillaries to be used could be glued before the final assembly was mounted into the reactor itself. This configuration thus removes the need for sealing fragile capillaries using ferrules and has been verified by us to be able to support temperatures up to 1273 K and elevated pressure operation (to ca. 18 bar) as per the original design. All measurements made with this reactor utilised a type K mineral insulated thermocouple inserted into the outlet of the sample bed.

Gases (argon, oxygen, and methane) were used in their pure forms and as supplied by the beamlines. However, to ensure gas purity upon delivery to the sample, they were passed through oxygen/water scrubbers (Supelco) equipped with bypasses as appropriate, prior to the mass flow control systems that controlled the flow of each gas at 20 mlmin⁻¹.

Ca. 10-20 mgs of sieved Cu/MOR sample was loading into the reactor in the form of a packed bed (see figure 1) secured at either side using quartz wool. The loaded sample was purged at ambient temperature using Ar and thorough leak checking made (using mass spectrometry and/or pressurization) of the system made.

Cu K-edge XAFS measurements were then made at room temperature (hydrated sample). The feed was then switched to oxygen and the sample was heated to 723 K at a rate of 10 Kmin⁻¹. Upon attaining 723 K the sample was allowed to remain at this temperature for 30 minutes before being

cooled at the rate permitted by the different reactors used. During this time XAFS spectra, indicative of the fully dehydrated Cu/MOR were collected.

We note herein a further significant difference between the air-blower systems and the bi-directional, resistive element, heating system exists that, whilst not affecting the measurements made in this study, does mean the duty cycles associated with repeated activation/reaction measurements are very different. The large thermal mass of the air-blowers means that cooling rates are limited if the heater is left in place whereas the resistively heated system cools back to the desired reaction temperature more rapidly and cooling rates of ca. 60 Kmin⁻¹ can be achieved. In this respect, the resistively heated reactor can also therefore be seen to be more time efficient.

Once cooled to reaction temperature (473 K) XAS spectra were again collected under flowing oxygen - as a verification that (spectroscopically) the sample had not changed during the cooling cycle - before feed was switched briefly to Ar, and then, to methane. The system was then allowed to develop under the methane atmosphere for a period of ca. 1 hour during which time Cu XAFS measurements were continuously collected.

At the end of the reaction, and where it could be verified that the systems was no longer changing, the samples were mapped using XAFS axially and radially (SNBL) or just radially (DUBBLE) to establish the spatial variations in Cu speciation present in the catalyst beds.

Lastly, in the case of the bi-directional heating system and post-reaction with methane, the sample was heated in 25 or 50 K steps to 723 K. At each temperature the system was monitored using XAFS and allowed to stay at that temperature until the spectra derived were observed no longer to vary. In this way the step-wise TPR shown in Figure 3 was derived and an internal standard arrived at for Cu^I. [31]

The resulting Cu K-edge XANES was normalised and linear combination (LCA) analysis was made using the Prestopronto software, [S3] to extract the levels of Cu^I and Cu^{II} present at the positions measured within the sample beds.

Standards for the LCA analysis were all derived internally from the sample: the XANES measured at room temperature (hydrated Cu^{II}); that measured after activation at 723 K and then again post cooling to 473 K (dehydrated (Cu^{II}); and lastly the XANES derived from subsequently heating the sample in a stepwise manner to 723 K (internal reference for Cu^I).

Infrared imaging was carried out in one of the off-line laboratories of ID15 at the ESRF and using an infrared camera supplied by the ESRF (VarioCAM, Infratec GmbH, Dresden), and data collected using Irbis 3.0 software.

3. Thermal assessment of other reaction cells.

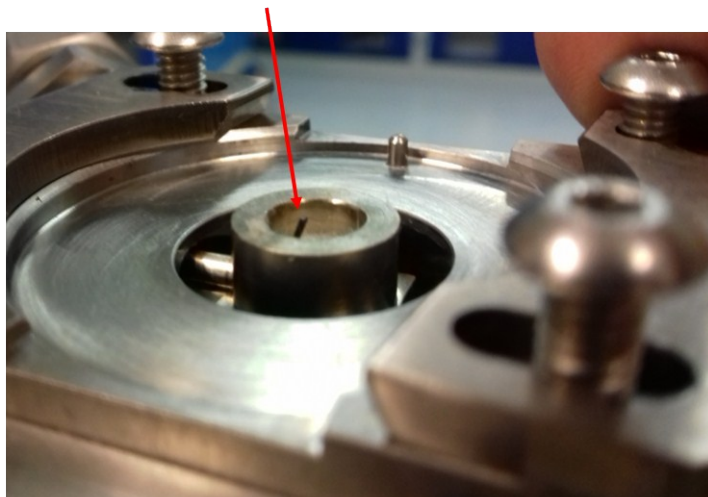
As a result of our studies a further two commercial reactor systems design for in situ measurement of materials using spectroscopies of different types (UV-vis, Raman, infrared, XAFS and XRD) were also interrogated. In the first case a Harrick cell (standard high temperature DRIFTS accessory for Paying mantis optics) fitted with a flat ZnSe window was subjected to investigation using the infrared camera; in a second case a further Harrick cell, adapted for combined infrared/XAFS/high energy X-ray scattering (ref. [42] main paper) was investigated using high energy XRD. The results of these investigations are given below as is a step-by-step example of how XRD measurements using a known material (in this case Ag powder), can be used to determine the temperature of a sample bed in situ. Whilst this procedure is, no doubt, well known within the crystallographic community, it is thought of utility to describe it here for the benefit of others.

3.1 Investigation of absolute temperature measurement and thermal gradients within a Flat-top Harrick spectroscopic cell.

In this study we aim to assess two aspects of this cell. Firstly, the accuracy of the thermocouples internal to the cell in reflecting the true temperature of the sample contained within

it and, secondly, the presence and nature of any radial thermal gradients that may exist across the 7 mm wide sample containing pan. The offline setup used to achieve this is shown in figure S1.

Thermocouple inserted from
Gas exit to measure surface T of bed



Ground Al_2O_3 bed; quartz wool underneath

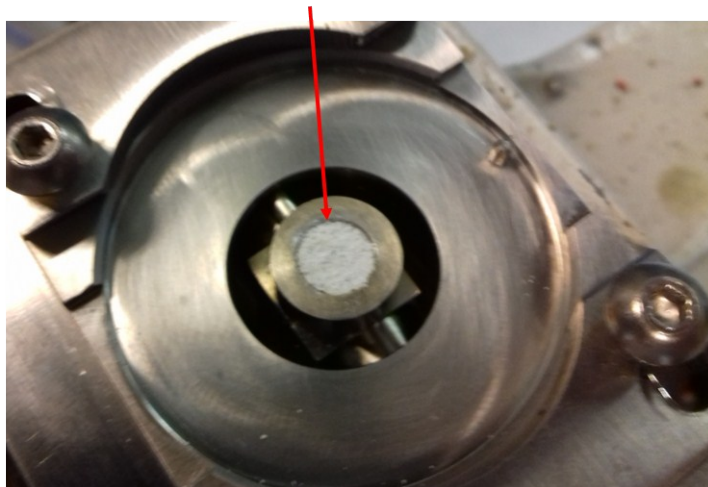


Figure S1. Flat top Harrick cell as setup for thermal imaging. Top panel shows the insertion of a type K mineral insulated thermocouple via the cell exhaust piping to arrive at top of the sample container. The bottom panel shows the sample container after filling with a ground alumina sample sat upon a loose plug of quartz wool.

The cell was placed under a flow of nitrogen (20 ml min^{-1}), and then imaged using the infrared camera from above at temperatures in the range of 298 K to 673 K. Restrictions in the availability

certain resources meant that these tests has to be conducted in the absence of a flow of cooling water.

Figure S2 shows the correlation obtained between the set point set using the control system – and as determined by the control thermocouple within the cell system – and the actual temperature of the bed as measured by the thermocouple seated within the bed (Figure S1).

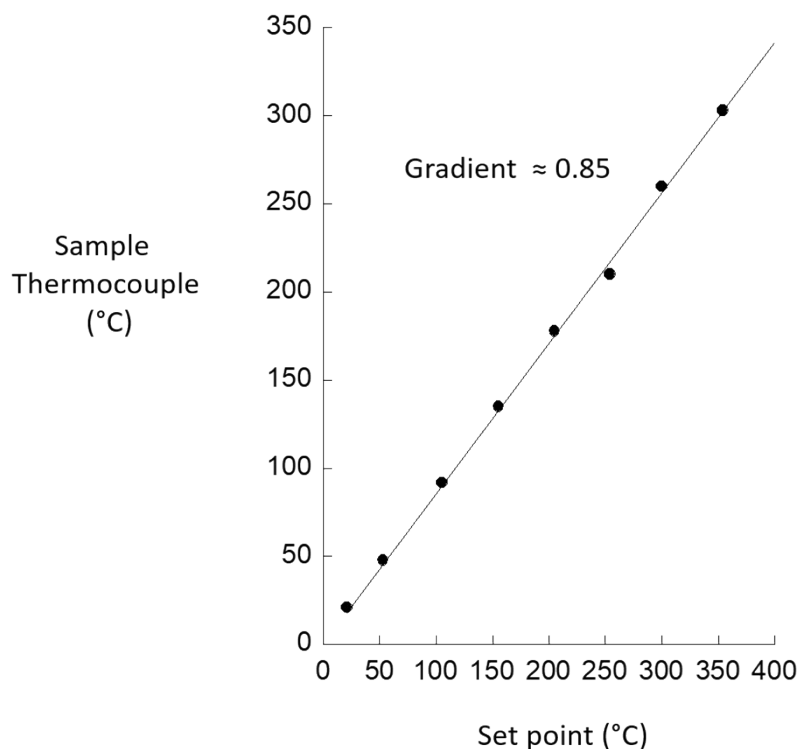
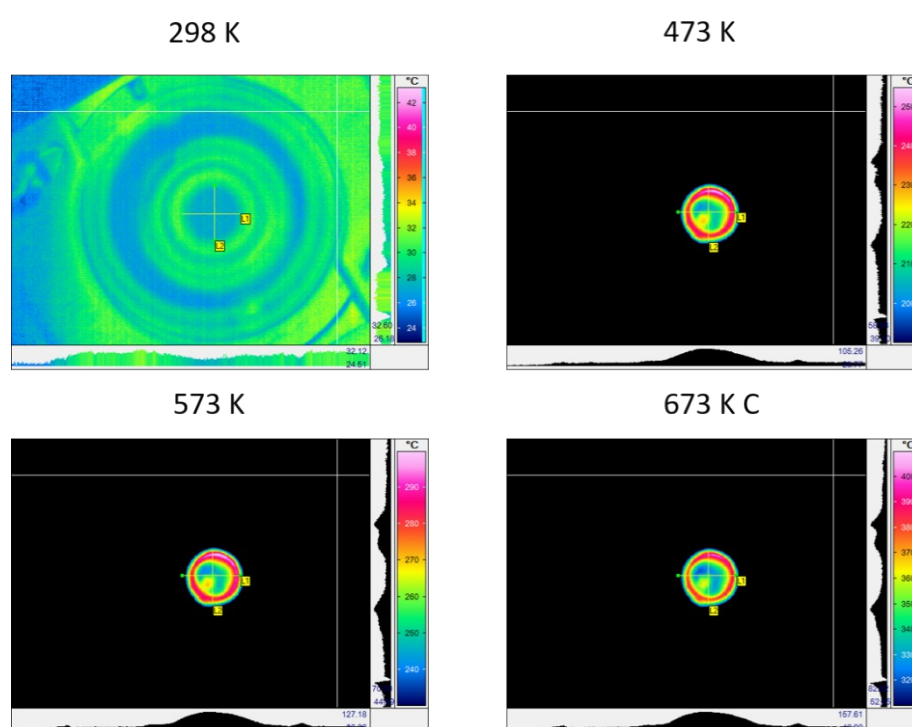


Figure S2. Correlation between the set-point temperature of the Harrick cell with that derived from the thermocouple inserted into the top of the sample bed as delineated in Figure S1.

A good linear relationship between the desired (set-point) temperature and the temperature as measured by the thermocouple is obtained. However, the gradient describing this linear relationship is not unity. Instead, a gradient of ca 0.85 is results from least squares fitting of the data. That is to say that across this range and under these measurement conditions the actual sample thermocouple returns a temperature 15% lower than that actually set. In the current instance this means that to achieve a reaction temperature in the surface region of the bed of 473 K (200 °C) a set-point of 503 K (230 °C) is indicated to be required. Correspondingly for the Cu/MOR system to be

activated at 723 K, although outside the range of the current study, this relation suggests that a set-point of ca. 577 °C would be required. This is extremely important to know in the current case. Copper zeolites must achieve full dehydration for the activation procedure to work and a true measure of its subsequent reactivity toward methane obtained; a failure to fully dehydrate all of the sample in this case will result in reactivity data that does not reflect the true behavior of the material.

Figure 3 then shows the results of infrared imaging obtained at four different temperatures



(as indicated).

Figure S3. Thermal (infrared) images of the Harrick flat top cell taken at four different set-point temperatures as indicated.

These images serve to illustrate a variety of aspects in regard to the thermal behaviour of this cell. The image taken at ambient temperature serves primarily to delineate the dimensions of the sample bed. In this case the different colours reflect the different emissivity of the materials present rather than any differentials in actual temperature. The subsequent images however show very clearly the thermal gradients that exist across the radial dimensions of the 7 mm diameter sample bed. We

can also see precisely where the thermocouple inserted into the surface region of the bed is present and that the packing of the sample around this element has caused it to be pushed a little to one side (to the left and down) of the sample bed.

The presence of the thermocouple is betrayed by a region of apparently higher temperature. Whether this is in fact a real thermal effect, one that arises from the sheath of the thermocouple conducting heat from the body of the cell to artificially warm the thermocouple itself, or, is the result of the higher emissivity of the stainless steel insulation of thermocouple relative to the alumina, however, is not clear.

What is clear, however, is that some significant radial temperature gradients within the sample bed are present at every temperature: the majority of the sample exists at a significantly lower temperature than indicated by the thermocouple save for an annulus near to the edges of the sample pan that appear significantly hotter.

These results would generally fit with previous measurements of similar types of systems (ref. [12], main paper) wherein it has consistently found, through other means, that the actual temperature of the samples in these sorts of cells was verifiably and considerably lower than the control systems would indicate. Whilst absolute precision is difficult to achieve in this measurement, it is however evident that this system cannot be considered as isothermal across its radial (surface dimensions) and both this, along with the absolute measurement of temperature in this case are potential sources of significant error in any attempt to derive quantitative structure function relationships. Moreover, our methods are not able to access the axial (depth) dimension of the sample bed and therefore any additional gradients that might exist in this direction remain unknown.

3.2 Investigation of ample temperature within a domed Harrick spectroscopic cell implemented for combined infrared/XRD/PDF measurements at ID15A, ESRF using high energy XRD.

The second additional cell we have investigated is a derivation of the standard Harrick DRIFTS cell. This cell has been modified such that infrared (DRIFTS) measurements may be performed in parallel with transmission X-ray method such as XAS, XRD and total X-ray scattering/PDF analysis probes. The version currently implemented at ID15 is a commercially available option derived from that originally designed and demonstrated by Beyer et al (ref. [42] main paper) at Sector 11 of the Advanced Photon source, USA ([ref [41], main paper). The central difference between this cell and the commercial cell discussed in the above section is the radial dimension of the sample holder is limited to 3 mm diameter. This derives from its desired implementation for high energy XRD and PDF measurements wherein any projection of the radial bed dimension onto the X-ray scattering data is must be minimal.

The question we ask here is whether either of the two thermocouple present in this cell (one in the heating block, hereafter called TC1, and one pressed into the metal surround of the sample container, hereafter called TC2), yield a good measurement of the actual sample temperature achieved in the upper part of the sample bed; it is in this first millimeter of the sample bed that the X-ray measurements are to be made and where most of the signal detected in DRIFTS is derived.

To achieve this we have used X-ray diffraction from silver powder (Goodfellow, 99.99%, max. particle size 45 μm); the following therefore also acts as an exemplar for those interested into how to derive sample temperature information from XRD.

The sample bed was packed with the Ag powder, the cell lid sealed, and Ar was flowed at 10 mL/min. The temperature controller (Eurotherm 2408) was locked to the reading of TC1. After the temperature was set to 300 K, the cell was allowed stabilise for 15 minutes. The readings of TC1 and TC2 were $T_1=302.7$ K and $T_2=300.0$ K, respectively. 2D diffraction images were acquired as the average of ten exposures of 0.8 s. The temperature was increased to 680 K, in 10 K increments, at a rate of 1 K/min. At each increment the system was allowed to stabilize for 10 minutes before XRD data was acquired. The Ag powder XRD images were radially integrated using FabIO and pyFAI [S4] and Rietveld-fitted using Topas v5 (Bruker-AXS, Karlsruhe, Germany). The background was fitted over all

the patterns by a 5-parameter Chebyshev polynomial. The line profiles were fitted by Thompson-Cox-Hastings functions [S5], whereby the Gaussian parameters and the mixing parameter η were refined over all patterns and the Lorentzian parameters were individual to each pattern. The cubic lattice parameters and the isotropic thermal parameters B were also refined independently for each pattern. The sample-detector distance (934 mm) and the X-ray wavelength (0.12398 Å) were calibrated on the pattern of CeO₂ (NIST 674B) collected in the same 3 mm sample bed.

Ag lattice parameter values were taken from Ref [S6]. We define the parameter ϵ as the lattice thermal expansion with respect to the value at 300 K, a_{300} : $\epsilon=(a(T)-a_{300})/a_{300}$. So the differential expansion da/dT is related to ϵ as follows:

$$\frac{da}{dT} = a_{300} \frac{d\epsilon}{dT} = a_{300} \alpha$$

The fit to the reference data (courtesy of D. Chernyshov) in Figure S4 (a) shows the validity of the cubic approximation of ϵ vs T in the temperature range used here. We therefore use the reference values from Mauer and Bolz [S6] to fit T as a function of ϵ with a cubic polynomial. Then the temperature increase corresponding to our observed lattice expansion is found by evaluating the polynomial over the experimental values of ϵ obtained from the Rietveld refinements between 300 K and 680 K. The error on the temperature calculated by propagating the uncertainties on the refined lattice parameters:

$$\delta T = \frac{1\delta a}{\alpha a} \sqrt{1 + \frac{a^2}{a_{300}^2}}$$

The values of ϵ , which depend entirely on the quality of the diffraction and the phase fits (the error on the fit of the reference data is negligible), are all between 0.7 and 1.2 degrees, or 0.2 and 0.3%.

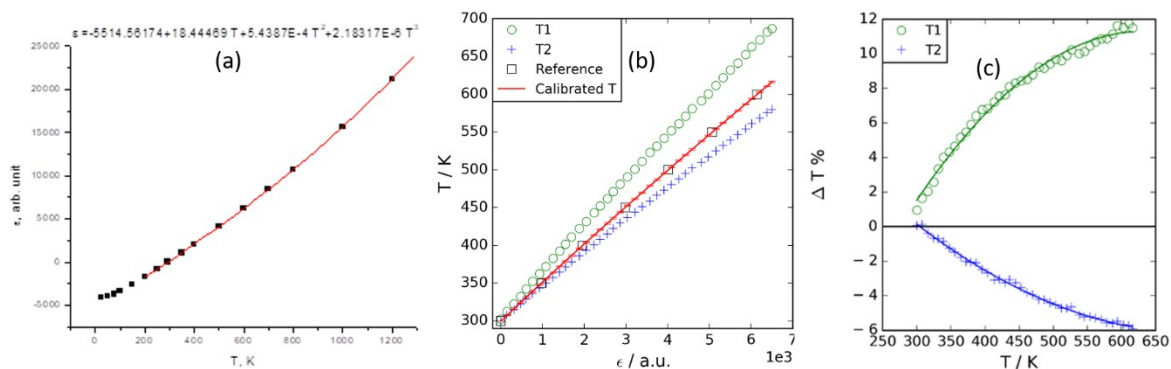


Figure S4. (a) Validity of the cubic approximation of ϵ vs T in the temperature range 300 – 680 K; (b) sample temperature as measured using XRD (red line) compared against the two thermocouples (T1 and T2) present within the sample mounting heating stage of the Harrick DRIFTS/XRD cell; (c) the percentage error between the sample temperature as determined by XRD and T1 (green) and T2 (blue).

The results shown in Figure S4 (b) and (c) make apparent (Figure S4 (b)) that the thermocouple placed in the heating block (TC1) significantly overestimates the sample surface temperature, whilst TC2, positioned outside, but much closer to the sample, underestimates the sample temperature. TC2 returns the value closest to the calibrated value of T as measured by XRD. Either way, however, and especially at more elevated temperatures, the difference between T1 and T2 and the sample temperature determined using XRD, is significant with this differential increasing with temperature. The different quadratic dependences shown in figure S4 (c) suggest that heat dissipates across two slightly different distances, i.e. from the heating block to the powder and from the powder to the edge of the sample bed.

Supplementary references.

[S1] W. van Beek, O. V. safonova, G. Wiker, H. Emerich, *Phase Transitions*, 2011, **84**, 726.

[S2] S. Nikitenko, A. M. Beale, A. M. J. van der Eerden, S. D. M. Jacques, O. Leynaud, M. G. O'Brien, D. Detollenaere, R. Kaptein, B. M. Weckhuysen and W. Bras, *J. Synchrotron. Rad.*, 2008, **15**, 632.

[S3] S. J. A Figueroa, C. Prestipino, *JPCS*, 2016, **712**, 012012

[S4] a) E. B. Knudsen, H. O. Sørensen, J. P. Wright, G. Goret, J. Kieffer, *J. Appl. Cryst.*, 2013, **46**, 537; b) G. Ashiotis, A. Deschildre, Z. Nawaz, J. P. Wright, D. Karkoulis, F. E. Picca, J. Kiefer, *J. Appl. Cryst.*, 2015, **48**, 510.

[S5] P. Thompson, D. E. Cox, J. B. Hastings, *J. Appl. Cryst.*, 1987. **20**, 79.

[S6] F. A. Mauer, L. H. Bolz, National Bureau of Standards, WADC-TR-55-473, 1.